Flexible Semitransparent Dual-electrode Hydrogel based Triboelectric Nanogenerator with Tough Interfacial Bonding and High Energy Output

Xin Jing[a], Heng Li[c], Hao-Yang Mi[a,b], Pei-Yong Feng[a], Xiaoming Tao[d], Yuejun Liu[a]*, Chuntai Liu[b], Changyu Shen[b]*

[a] Key Laboratory of Advanced Packaging Materials and Technology of Hunan Province, Hunan University of Technology, Zhuzhou, 412007, China

[b] Key Laboratory of Materials Processing and Mold, Zhengzhou University, Zhengzhou, 450000, China

[c] Department of Building and Real Estate, Hong Kong Polytechnic University, Hong Kong, 999077, China

[d] Institute of Textile and Clothing, Hong Kong Polytechnic University, Hong Kong, 999077, China

Corresponding Authors:

H.Y. Mi E-mail: mihaoyang@zzu.edu.cn
Y. Liu E-mail: yjliu_2005@126.com

Note:

The authors declare no competing financial interest.

Abstract:

Triboelectric Nanogenerators (TENG), as a novel technique that is capable to harness ubiquitous mechanical energy, has gained tremendous attention in recent years. Developing flexible and transparent TENG with high triboelectric output performance is a major challenge towards adaptable and invisible energy harvesters. Previous developed transparent TENGs are normally in single electrode working mode or have relatively low output. Herein, a flexible semitransparent dual-electrode hydrogel-based TENG (DH-TENG) with high output was developed. The DH-TENG contains thermoplastic polyurethane (TPU) tribopositive layer and polydimethylsiloxane (PDMS) tribonegative layer. Both materials are highly transparent. NaCl containing polyacrylamide (PAM) hydrogel was used as electrodes, and polyethylene terephthalate (PET) sheets were used to provide mechanical stiffness. A benzophenone (BP) grafting method was used to enhance the interfacial bonding between hydrophobic triboelectric materials and hydrophilic hydrogels, which realized a significant improvement of tear strength of over 12 times. The DH-TENG demonstrated a high instant voltage and current of 311.5 V and 32.4 μA respectively. A maximum power density of 2.7 W/m^2 was achieved on a 4.7 MΩ resistor. Furthermore, the DH-TENG showed a highly stable output in continuous running, and demonstrated capability to charge capacitors, and power small electronics such as a timer, pedometer, and digital watch.

Keywords: Triboelectric nanogenerator; Hydrogel; Transparent; Interfacial bonding; Energy harvesting

1. Introduction

The invention of triboelectric nanogenerators (TENG) in 2012 opened a new ear for ubiquitous mechanical energy harvesting and green energy generation. [1, 2] The inherent simple device composition and small unit size make TENG a much-anticipated energy source for portable and wearable devices. [3] When compared to other energy harvesting methods, such as hydroelectric, photovoltaic, and piezoelectric generation methods, TENGs generally have higher output voltage and power density, low fabrication cost, and high energy conversion efficiency.[4-6] Nevertheless, more challenges are raised for wearable TENGs that are desired to become lighter, flexible and even transparent to be effectively integrated onto human body and improve experience feeling.

Extensive efforts have been made in the last few years to develop transparent and flexible TENGs by using transparent and flexible triboelectric materials and electrodes. [7-10] In a typical TENG device, materials with opposite triboelectricity were contacted and separated repetitively to induce charges transfer based on the coupling effects of contact electrification and electrostatic induction. [11, 12] Thus a dynamic electrostatic potential difference between the two materials is created which further leads to the flow of electrons in the external circuit. Since the triboelectric materials are usually insulators, electrodes (or current collectors) with high conductivity are often required to induce the current flow in the external circuit. Transparent triboelectric materials such as polydimethylsiloxane (PDMS) [13], poly(vinyl alcohol) (PVA) [14], and polyethylene terephthalate (PET) [15] have been used for TENG fabrication. Among all triboelectric materials, PDMS is the most frequently used tribonegative material due to its excellent transparency and flexibility. [16, 17] However, the available choice for high performance transparent tribopositive material is very limited because most tribopositive materials are opaque. In most cases, the TENGs were fabricated in single-electrode mode and the external circuit is grounded. Theoretically, single-electrode

TENG only possesses half output compared to dual-electrode TENG made of the same materials.[18, 19] Moreover, the energy output of single-electrode TENGs is heavily dependent on the triboelectivity of the material they are in contact with. This greatly limits their applicability as well as their stability. However, the fabrication of dual-electrode TENG with high transparency is challenging since the refraction caused by the air layer between tribopositive layer and tribonegative layer will reduce the device transparency as well. [7] Therefore, how to fabricate Dual-electrode TENGs with relatively high transparency and high output is an ongoing challenge.

The property of electrodes is another critical factor affecting the flexibility and transparency of TENG. Coating a thin layer of conductive material, such as poly(3,4-ethylene dioxythiophene) (PEDOT) [20], graphene [21], and silver nanowires [22], on triboelectric layers is a straight forward way to fabricate transparent electrodes for TENG. However, the poor stretchability of the conductive coating may lead to permanent performance deterioration under repetitive mechanical deformation.[23, 24] Recently, ionic conductors have been recognized as good candidates for TENG electrodes attributing to their superior conductivity, transparency, flexibility, as well as self-healing ability. [25-27] Pu et al. developed an ultrastretchable, transparent single-electrode TENG using stretchable 3M VHB tape as triboelectric material and polyacrylamide (PAM) hydrogel containing lithium chloride (LiCl) salt as the ionic conductor. [28] Similarly, Lee et al. fabricated a stretchable, transparent and self-healable single-electrode TENG using crosslinked PVA gel as ionic current collector, silicon rubber as triboelectric negative material, and VHB tape as the substrate. [29] Zhao et al. fabricated an ionogel-PDMS based TENG that is capable to detect tactile forces. The TENG is composed of transparent ionogel as both tribopositive layer and electrodes, and patterned PDMS as tribonegative layer. [30] Although the ionogel based TENG works in dual-electrode mode, its output performance is relatively low.

The delamination of ionic conductor and triboelectric layer upon mechanical deformation is a critical issue when ionic conductors are used as electrodes. This is because of the low compatibility between the ionic material and triboelectric elastomer. [4] Various packaging techniques were developed to tightly confine the hydrogel electrode, while the poor interfacial bonding remains unresolved. Wang et al. first introduced benzophenone (BP) modification in hydrogel based TENG fabrication to enhance the interfacial bonding between hydrophilic ionic layer and hydrophobic PDMS. [31, 32] The modification process was simple and did not affect the transparency of TENG. So far BP modification has been used in several studies, while most current efforts have been focused on PDMS and single electrode TENGs. [8, 33, 34] Developing robust dual-electrode transparent and flexible TENG with high output is still a challenge.

In this study, a flexible DH-TENG with moderate transparency and stable high energy output was developed using thermoplastic polyurethane (TPU) as tribopositive layer, PDMS as tribonegative layer, and PAM hydrogels as ionic electrodes. BP was successfully used to enhance the interfacial bonding of PAM hydrogel to both TPU and PDMS. The developed DH-TENG maintained a transmittance of about 56%, and delivers a high output voltage of 311.5 V and an output current of 32.4 μA. A maximum power density of 2.7 W/m^2 was achieved on a 4.7 MΩ external load. The DH-TENG was able to operate stably at high frequency of 20Hz and the energy generated was successfully stored and used to power small electronics such as a timer, pedometer, and digital watch.

2. Experimental Methods

2.1 Materials

TPU (1185A, M_w =109 kDa by GPC) was purchased from BASF. PDMS kit (Sylgard TM 184) was purchased from Dow Corning Company. Chemicals and reagents including

acrylamide (AM), methylene bisacrylamide (MBA), ammonium persulfate (APS), BP, NaCl, and tetramethylethylenediamine (TEMED) were purchased from Sigma-Aldrich. All reagents were used as received. Milli-Q deionized water was used through all experiments.

2.2 Preparation of TPU and PDMS triboelectric layers

TPU triboelectric layer was prepared by hot compression of pre-dried TPU pellets in a rectangular mold 50 × 50 × 1 mm at 180 °C under 5000 psi for 5 min. Then the TPU sheet was further compressed at 150 °C under 2500 psi for 1 min to produce a thin TPU film with thickness of 200 μm. PDMS film was produced by fully mixing the base and crosslinker at a weight ratio of 10:1, followed by spin coating on a polystyrene (PS) plate at 1000 rpm for 1 min and curing at 60 °C for 2h. The obtained PDMS film also has a thickness of 200 μm.

2.3 Synthesis of PAM hydrogel layer

To prepare the PAM precursor solution, 2.84 g AM, 1.7 mg MBA, 4.8 mg APS, and 117 mg NaCl were dissolved in 20 mL DI water, followed by addition of 7.1 mg TEMED. Once all chemicals were fully dissolved, 10 mL solution was poured into a PS Petridis followed by UV crosslinking for 40 min. The obtained PAM hydrogel has a thickness of 1 mm.

2.4 BP modification for TPU and PDMS

The surface of TPU film was treated by BP in ethanol solution based on the following procedure. First, the surface of TPU film were cleaned in methanol and deionized water carefully, followed by soaking into the prepared BP solution (10% wt. in ethanol) for 5 min at room temperature. After that, the treated surface was washed with methanol thoroughly and dried with nitrogen gas. Then, the PAM hydrogel film was placed on to the surface of TPU, followed by UV treatment (in the UV chamber, 350 nm ultraviolet) for 1 h, during which time, the PAM hydrogel network was covlently crosslinked and bonded to the TPU elastomer surface. The BP modification for PDMS followed the same protocol. The BP solution concentration and treatment time were optimized in our preliminary study as provided in the supporting information (Figure S1).

2.5 Fabrication of dual-electrode hydrogel based TENG (DH-TENG)

Both TPU/PAM layer and PDMS/PAM layer were attached to polyethylene terephthalate (PET) films with thickness of 0.2 mm and sealed using epoxy glue to form the positive and negative layers in the DH-TENG device. An air gap was created by placing PDMS spacers (height of 2 mm) between the positive and negative layers. PET films were used to enhance the mechanical stability of the dual-electrode H-TENG, and maintain a air gap between the two layers, since the TPU film, PDMS film and PAM hydrogel are all highly flexible material. The edges of the DH-TENG were confined using polyethylene tape.

2.6 Characterization methods

The peeling of PAM hydrogel from the attached PDMS or TPU films was observed using an optical microscope (Nikon Eclipse Ti-S) to reveal their interfacial bonding behavior. The adhesion strength was measured by tear test on a universal mechanical tester (Instron 5967, USA, 250 N load). The hydrogel and substrate were pulled at a cross head speed of 5 mm/min until the hydrogel detach from the substrate. The maximum force during measurement was recorded as the tear strength. The transparency of tribopositive, tribonegative and DH-TENG was measured using a UV-vis spectrophotometer (Cary 500 UV-vis-NIR spectrophotometer) in the range of 800 to 200 nm with blank reference. The triboelectric output performance of the DH-TENG was evaluated by compressing using a dynamic shaker (Shiao, SA-JZ) with controlled force and frequency which were regulated by a signal generator (BK Precision, 4003A) and a signal amplifier (Yamaha, A-S201). The output voltage was recorded using an oscilloscope (ZDS3034 Plus) and the output current signal was recorded using a potentiostat (CHI760E).

3. Results and Discussion

The DH-TENG developed in this study is composed of two composite triboelectric layers and an air gap between them. As illustrated in Figure 1a, the tribopositive layer is composed of a TPU film, a PAM hydrogel, and a PET film, while the tribonegative layer contains a PDMS film, a PAM hydrogel, and a PET film. The PET films were used to provide mechanical stiffness so that the air gap can be regained after the DH-TENG is compressed. The NaCl containing PAM hydrogels were used as transparent electrodes that induce the current flow in the external circuit. The electrostatic potential difference created between the upper and lower hydrogel electrodes is highly dependent on the charges generated on triboelectric films as well as the interfacial bonding between the hydrogel and triboelectric films. Unfortunately, the attachment of TPU and PDMS with hydrogel is generally low because they have significantly different surface energy and wettability.[35, 36] In order to increase the interfacial bonding between triboelectric material and PAM hydrogel, BP was used to create covalent bonding between the triboelectric material and the PAM hydrogel. As shown in Figure b, BP could induce hydrogen atom transfer under UV irradiation, which could create free carbon radicals on TPU, PDMS, and PAM chains. These free carbon radicals can further react with each other to form covalent bonds, and thus enhance the bonding force between hydrophilic PAM hydrogel and hydrophobic TPU and PDMS films. [31, 37, 38] The BP bonding efficiency was investigated by optical microscope, and tear test. It was found that PDMS film has very low adhesion to PAM hydrogel without BP modification. The hydrogel can be easily peeled off and no sticky behavior was observed on the interface during peeling as shown in Figure 1c. On the contrary, the adhesion between PDMS and PAM hydrogel with BP modification was significantly enhanced indicated by the sticky peeling behavior and the fibrils formed during peeling (Figure 1d). These fibrils implied the strong bonding between two materials and the formation of linkages. Similarly, the adhesion between TPU film and

PAM hydrogel was enhanced by BP modification as well, and sticky fibrils were also observed during peeling as compared in Figure 1e and f. The tear test verified that after BP modification the tear strength of PDMS and TPU to PAM hydrogel was significantly increased by over 12 times as shown in Figure 1g. It was found that the bonding between TPU and PAM hydrogel (2.21 N) was stronger than the bonding between PDMS and PAM hydrogel (1.67 N) indicated by greater tear strength. Thus, the introduction of BP crosslinking was highly effective in promoting the interfacial bonding between the conductive hydrogels and the triboelectric layers.

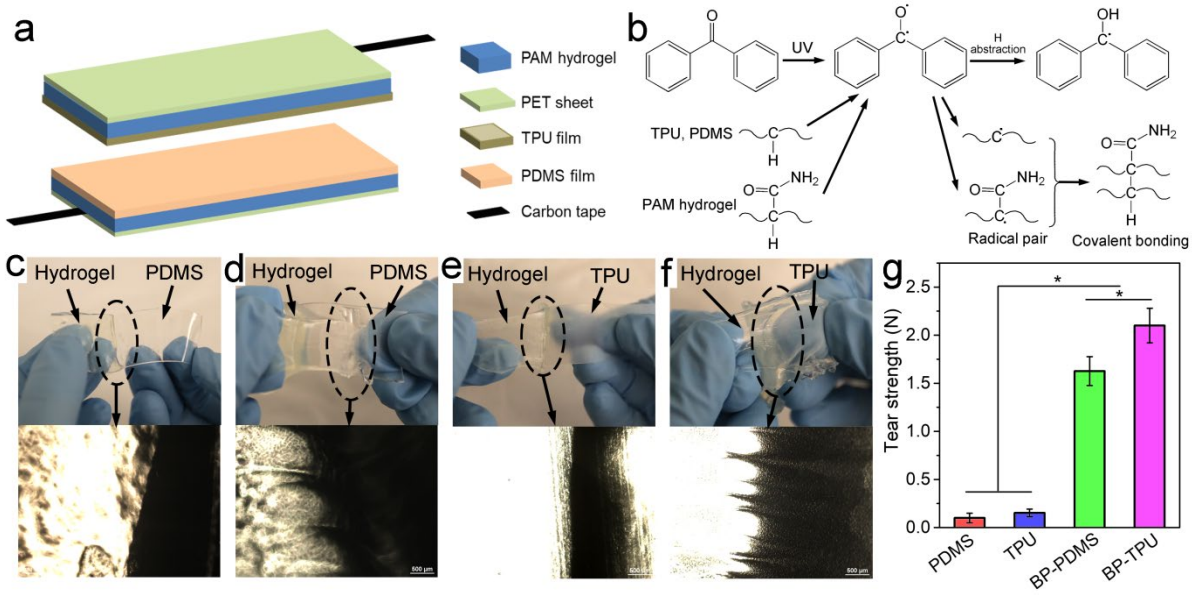

Figure 1. (a) Schematic illustration of the DH-TENG developed in this work. (b) Bonding mechanism of using BP to crosslink TPU and PDMS with hydrogel. (c-f) Digital photos and optical images showing the peeling and the interfacial bonding of hydrogel layers and triboelectric layers. (g) Tear strength of PAM hydrogel attached to PDMS layer and TPU layer with and without BP modification.

Figure 2a shows the digital photographs of the fabricated tribopositive TPU layer tribonegative PDMS layer, and the assembled DH-TENG. The two triboelectric layers were tightly packed and transparent. Conductive carbon tape was used as current lead to connect to

the external circuit. Four PDMS spacers were used to maintain an air gap between the two layers so that the DH-TENG can work in a contact-separating mode. As illustrated in Figure 2b, the mechanical stiffness provided by PET sheets is suitable to provide enough force to allow fast recovery of the DH-TENG when the compressing force is removed. From the UV-vis results (Figure 2c), it was found that the PDMS tribonegative layer has a transmittance of about 93% at 700 nm wavelength, the TPU tribopositive layer has a transmittance of about 83 %. The transmittance of pure PDMS is over 90 % and it is over 80% for pure TPU in wide wavelength range. The transmittance was reduced after overlapping with the hydrogel and PET films mainly due to the refraction and reflection on the interfaces. The transmittance of the assembled DH-TENG was decreased to about 56% at 700 nm wavelength. The significant decrease of transparency of the DH-TENG was mainly caused by the refraction of the air gap between the two layers. With the moderate transparency, one can still clearly observe the text beneath the DH-TENG.

The working principle of the DH-TENG is depicted in Figure 2d. The DH-TENG works in a contact-separating mode, in which charges were generated when the TPU layer is in contact with the PDMS layer due to the difference of their triboelectric properties. When the two layers are separating, a potential difference is created between them, which lead to the separation of cations and anions in the hydrogel electrodes. As illustrated in Figure 2d anions tend to move towards the TPU side and cations tend to move to the opposite side in the upper tribopositive layer, while the trends are opposite in the bottom tribonegative layer. This further causes the movement of electrons from the bottom layer to the upper layer in the external circuit, which induces an instant current flow through the external load. During the contacting period, the potential difference between the two layers is compensated as the two layers are approaching each other. [39] This will lead to a current flow in the opposite direction due to the redistribution of ions in the hydrogel electrodes. [40, 41] Therefore, the energy from mechanical motion is transferred to periodic electrical energy.

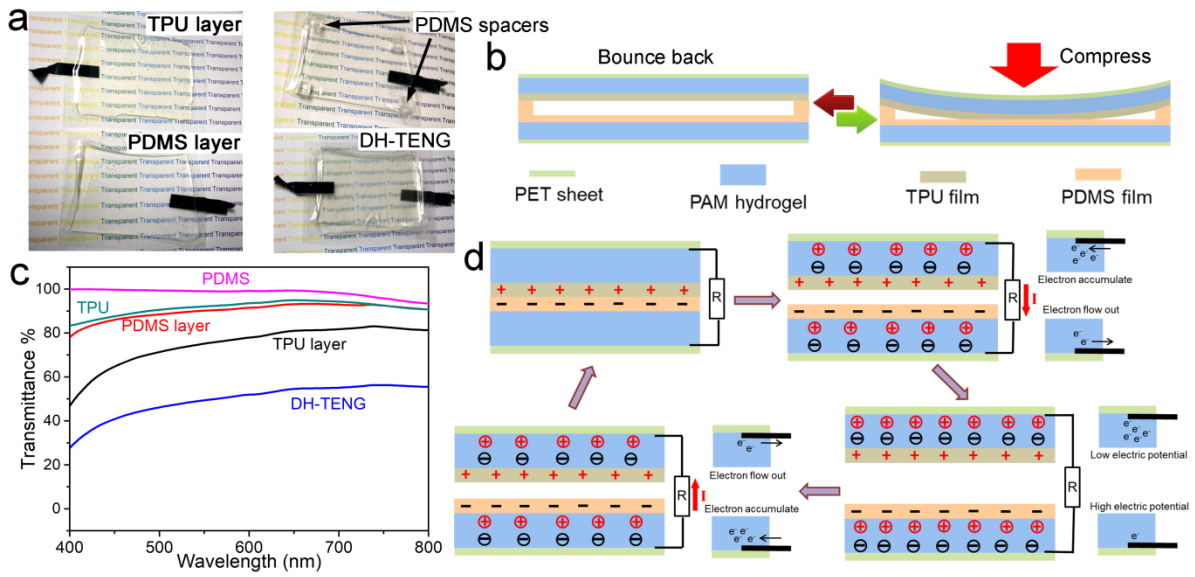

Figure 2. (a) Digital photographs showing the TPU layer, PDMS layer, and the assembled DH-TENG. (b) Illustration of the contact-separation working mode of DH-TENG. (c) UV-vis transmittance results of PDMS, TPU, PDMS layer, TPU layer and the DH-TENG. (d) Schematic illustration of the working principle of the DH-TENG.

Figure 3a shows the output voltage of the fabricated DH-TENG measured using an oscilloscope. A maximum instant voltage of 311.5 V can be achieved when the DH-TENG is compressed with a 6 N periodic force at 10 Hz. The instant positive voltage of 311.5 V is obtained in the pressing cycle, and the instant negative voltage of 158.5 V was achieved in the release cycle (Figure 3d). It is believed that the reason for the greater voltage in the pressing cycle than the releasing cycle is because the pressing force was greater than the bouncing force. [42] In order to investigate the triboelectric property of the TPU layer and PDMS layer, they were separately pressed against aluminum foil and the voltage signals were shown in Figures 3b and c. It was found that the PDMS layer showed a maximum positive voltage of 113.4 V, which means the PDMS gains electrons when it is in contact with aluminum. However, the TPU layer showed a maximum negative voltage of 36.8 V when compressed against aluminum, which implies that TPU loses electrons when it is contacted with

aluminum. Thus, the combination of PDMS layer and TPU layer caused a higher output voltage due to the high tribopositivity of TPU and tribonegativity of PDMS. The output current of the fabricated DH-TENG was measured using a potentiostat, it was found that the output current showed the same pattern with the voltage, and the maximum instant current of 32.4 μA was achieved (Figure 3e). In the continuous operation test (Figure 3f), the DH-TENG was continuously compressed for 30 min at 10 Hz. The output voltage signal was highly stable during the whole period indicating the DH-TENG possesses high long term stability. On the contrary, if the DH-TENG were assembled without BP modification, the low interfacial bonding between the triboelectric material and PAM hydrogel would lead to vibration and slipping of PAM hydrogel during repetitive compression, which would result in lower and less stable energy output. As shown in Figure S2, the output voltage and current of unmodified DH-TENG were ~285 V and ~25μA, respectively. When operated in long-term, significant output reduction was realized for the unmodified DH-TENG due to the ineffective contact caused by the slipping of PAM hydrogel (Figure S3). Therefore, the greatly enhanced interfacial bonding between triboelectric materials and PAM hydrogel is highly effective for improving the output performance and stability of the DH-TENG.

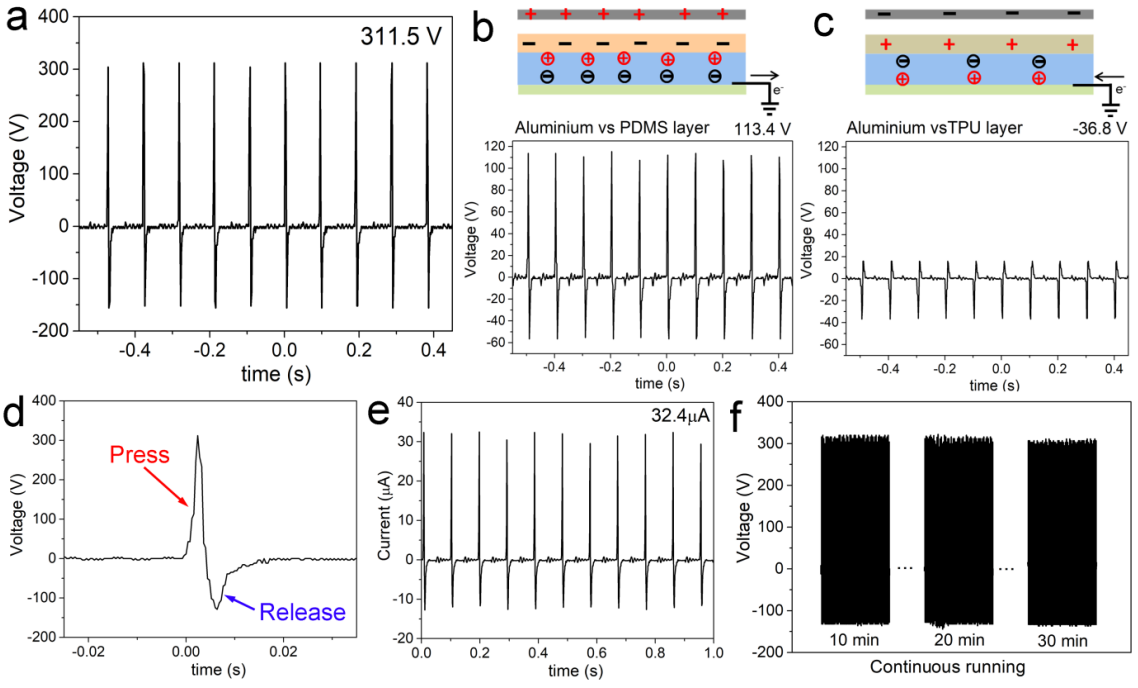

Figure 3. (a) Triboelectric output voltage signal of the fabricated DH-TENG; Output voltage signal of the (b) PDMS layer and the (c) TPU layer when pressed using aluminum; (d) High resolution output voltage signal in one pressing and releasing cycle; (e) Output current signal of the fabricated DH-TENG; (f) Output voltage signal of DH-TENG when continuous operating for 30 min at 10 Hz.

In order to further evaluate the performance of the developed DH-TENG in the external circuit, it was connected to a series of resistors with resistance range from 10 kΩ to 10MΩ. As shown in Figure 4a, the current density on the external load decreased slightly when the resistance was lower than 470 kΩ. When the resistance is further increased, the current density decreased rapidly due to the significant energy consumption on the resistor. The instant voltage on the resistor showed a gradual increasing trend as the increase of resistance of external resistor, and a maximum voltage of 110 V was achieved on a 10 MΩ resistor. The corresponding power density results showed that the power density gradually increased as the increase of external load resistance, and a peak power density of 2.7 W/m^2 was achieved on a 4.7 MΩ resistor. The power density achieved by the DH-TENG exceeded most hydrogel based TENGs, due to the significantly enhanced interfacial bonding strength and the dual-electrode structure. The properties of the DH-TENG were compared with flexible TENGs developed recently. As shown in Table 1, single electrode TENGs are easy to be fabricated with high transparency, but they usually have relatively low power density and output performance is highly dependent on the material in contact with them. Dual-electrode TENGs have more stable energy output, while high transparency is difficult to achieve due to the refraction of the air gap. The power density of the DH-TENG developed in this study exceeded majority transparent TENGs and the external loads required to obtain the maximum power density was lower than most of the TENGs. The high power density of DH-TENG should be high enough to be used as power sources for many electronics.

Table 1. Comparison of the DH-TENG developed in this study with flexible TENG reported in literature.

No	Materials	Working mode	Transmittance	Max. voltage	Power density	Ref.
1	PDMS, PAM hydrogel	Single electrode	~87%	71V	135 mW/m^2 (800MΩ)	31
2	VHB tape, carbon grease	Single electrode	None	115 V	N/A	41
3	Silicon rubber, PVA/polydopamine/CNT hydrogel	Single electrode	None	95V	750 mW/m^2 (500MΩ)	43
4	PDMS, Ag nanowire	Single electrode	96%	66V	446 mW/m^2 (71MΩ)	22
5	Cellulose nanofibril, phosphorene	Single electrode	64%	5.2V	1.06 μW/cm^2 (1MΩ)	44
6	PVA hydrogel, silicon rubber	Single electrode	92%	50V	40 μW/cm^2 (1MΩ)	29
7	Grapheme, PDMS, PET	Single electrode	44.5%	5V	N/A	10
8	VHB tape, PAM hydrogel	Single electrode	96.2%	145V	35mW/m^2 (7MΩ)	28
9	PDMS, Ionogel	Single electrode	90%	117V	1.3W/m^2 (10MΩ)	9
10	PVA/PEI hydrogel, PDMS,	Single electrode	83%	70V	2.79 W/m^2 (150MΩ)	34
11	ITO coated PET, PDMS	Dual electrode	~78%	200 V	1.1W/m^2 (10MΩ)	45
12	Graphene, PET	Dual electrode	97%	10V	2.5 μW/cm^2 (10MΩ)	46
13	ITO coated PET, PDMS	Dual electrode	83%	3.8V	0.75mW/m^2 (50MΩ)	47
14	ITO coated PET, PDMS	Dual electrode	~75%	18V	N/A	48
15	ZnO, ITO coated PET, PDMS	Dual electrode	63%	5.3V	N/A	49
16	H-PDMS, Ag nanowire, PEDOT	Dual electrode	67%	94V	327 mW/m^2 (400MΩ)	23
17	PDMS, PAMPS ionogel	Dual electrode	83%	1.4V	N/A	30
18	photopolymer resin, PAAm hydrogel	3D multilayer structure	none	68V	10.98 W/m^3 (0.75TΩ)	50
19	TPU, PDMS, PAM hydrogel, PET	Dual electrode	56%	311.5V	2.7 W/m^2 (4.7MΩ)	This work

The stability of DH-TENG output was investigated under different compress frequency range from 2 Hz to 20 Hz. As shown in Figure 4c, the output voltage was slightly higher when the DH-TENG was operated under high frequency, while the signal was maintained

stable under the same frequency. It is believed that the lower voltage at low frequency was caused by the smaller acceleration and impact force upon contact at low frequency due to the sinusoidal move of the shaker head. The output current signal showed the same trend with the voltage signals when the DH-TENG is operated at different frequencies (Figure 4d). According to the working principle of the DH-TENG, the electric signal generated is alternative, which is undesirable as an energy source for small electronics. Thus, the TENG is typically connected to a bridge rectifier in order to make use of the energy generated. Figure 4e shows the equivalent circuit to convert negative electric signals to positive signals. As shown in Figure 4f and g, the negative voltage was successfully converted to positive voltage through the bridge rectifier. It was found that the peak voltage was 305 V of the rectified signal, which is lower than the original voltage (311.5 V). This indicates energy was consumed in the bridge rectifier circuit, while the energy loss was only 2.1%.

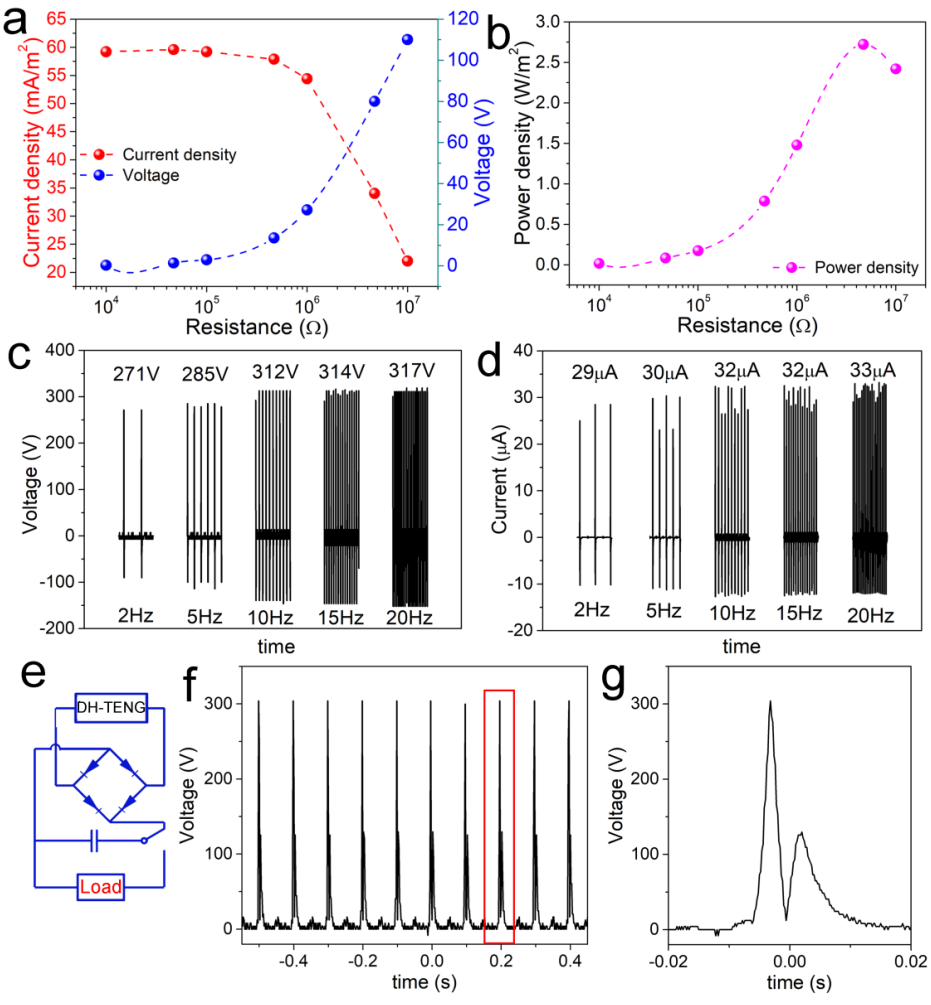

Figure 4. (a) The current density and voltage results (b) The power density of the DH-TENG when connected to external loads; (c) The voltage signal and (d) the current signal of the DH-TENG when pressed at different frequencies; (e) Equivalent circuit of the DH-TENG when connected through a bridge rectifier; (f) Rectified voltage signal using bridge rectifier, and (g) rectified voltage signal in one pressing and releasing cycle.

In order to make use of the energy generated, the DH-TENG was used to charge different capacitors through the bridge rectifier. Then the stored energy was used to power small electronics. As shown in Figure 5a, the DH-TENG fabricated was able to charge various capacitors. It can charge 6.8 μF, 10 μF, and 22 μF capacitors to 5 V in 58.8 s, 76.3 s, and 189.5 s, respectively. Next, the energy harvested can be used to power small electronics. As shown in Figure 5b and Movie 1, the energy stored in a 6.8 μF capacitor was able to power a digital timer when been charged to ~6V by the DH-TENG. However, the stored energy is not enough to continuously power the digital timer. The watch is diminished in a few seconds. The capacitor needs to be charged again to a higher voltage, and thus the timer can be powered periodically. In order to prolong the device operation time, a capacitor with larger capacitance (1000 μF) was used to store the energy generated by the DH-TENG. It takes about 30 min to charge the 1000 μF capacitor to 2 V, and the energy is sufficient to power a pedometer for over 10 minutes (Figure 5c and Movie 2). As shown in Figure 5d, the voltage had a small drop when the capacitor is connected to the pedometer, then the voltage is gradually decreased as the pedometer operates. Similarly, the 1000 μF capacitor charged by the DH-TENG was used to power a digital watch (Figure 5e and Movie 3). From the corresponding voltage results (Figure 5f), it was found that a sharp voltage drop of ~ 1V occurred to initiate the digital watch. After that, the watch is continuously been powered and the energy consumption is slightly faster than the charging rate by the DH-TENG. These demonstrations indicated that the DH-TENG fabricated is capable to be used to convert

mechanical motion into electrical energy and power small devices at high efficiency. Given the moderate transparency and high flexibility of the developed DH-TENG, it is capable to be used in diverse applications for mechanical energy harvesting without significantly affects the optical properties. Moreover, the energy output could be further enhanced by enlarging the area of the DH-TENG device or by stacking multiple DH-TENGs. Therefore, the developed DH-TENG is promising for portable and self-powered next-generation devices.

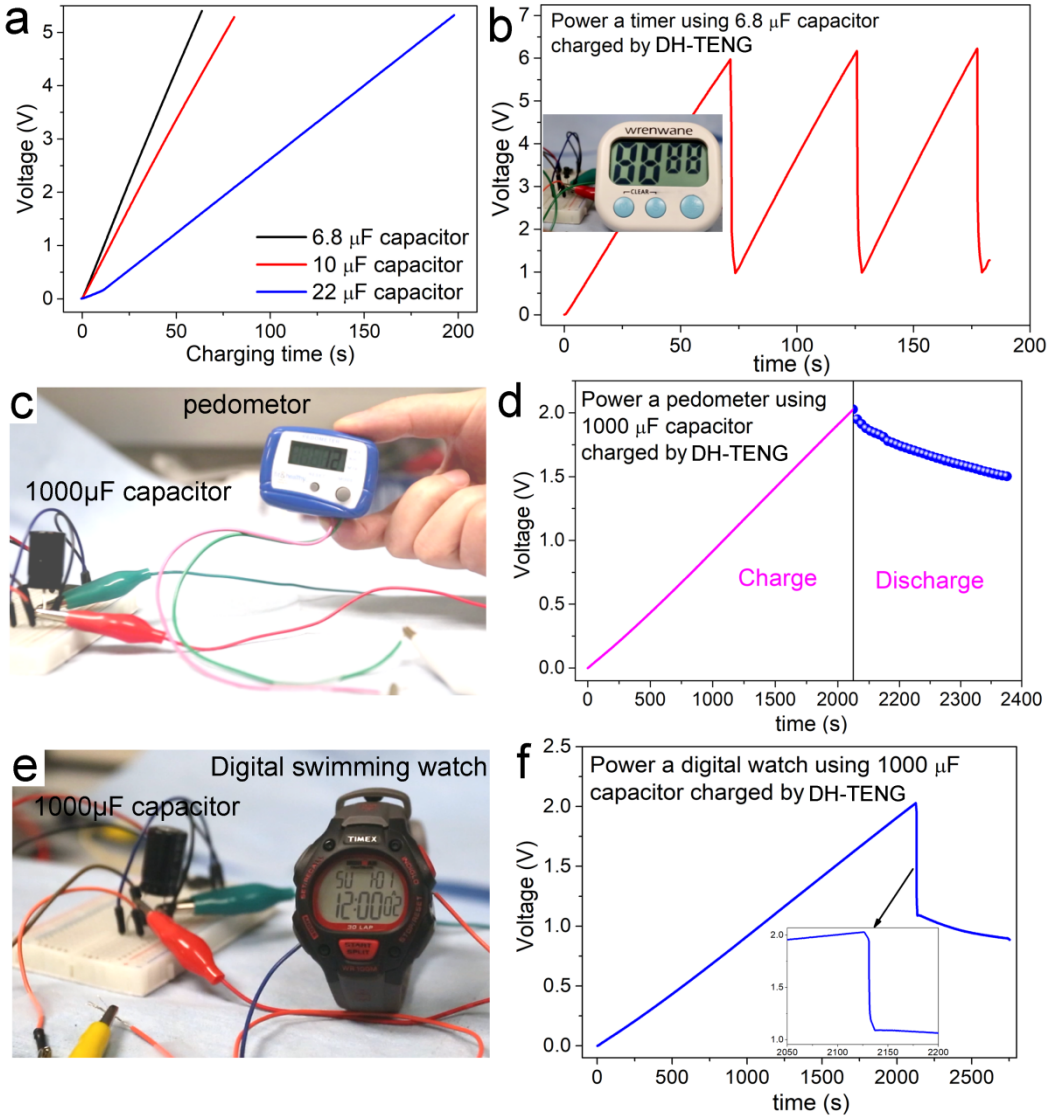

Figure 5. (a) Charge capacitors with different capacitance using the DH-TENG; (b) Power a digital timer using a 6.8 μF capacitor charged by DH-TENG; (c) Digital photo and (d) relevant voltage signal of a pedometer powered using a 1000 μF capacitor charged by DH-

TENG; (e) Digital photo and (f) relevant voltage signal of a digital watch powered using a 1000 μF capacitor charged by DH-TENG.

4. Conclusion

A new dual-electrode hydrogel based TENG (DH-TENG) with high flexibility and moderate transparency was developed in this study. The DH-TENG uses transparent TPU as tribopositive layer, PDMS as tribonegative layer, and NaCl containing PAM hydrogel as electrode layer. BP modification was used to enhance the interfacial bonding between hydrophobic TPU and PDMS to hydrophilic PAM hydrogel. The tear strength was improved by over 12 times with BP modification for both TPU and PDMS layers. The developed DH-TENG maintained a moderate transmittance of ~56 %, and a remarkable energy output performance. A high instant voltage of 311.5 V and an instant current of 32.4 μA were achieved by the DH-TENG. The maximum power density of 2.7 W/m^2 was achieved on a 4.7 MΩ resistor, which is the highest power density reported for hydrogel based TENG so far. Moreover, the DH-TENG showed a highly stable output in continuous running due to the strong interfacial bonding and dual-electrode structure. Attributing to stable high performance, the DH-TENG was able to quickly charge capacitors with various capacitances through a bridge rectifier, and thus be used as power source for small electronics such as timer, pedometer and digital watch. Therefore, this study provides a pathway to fabricate high performance semitransparent dual-electrode hydrogel based TENG, and demonstrates its potential application as an effective energy harvester.

Acknowledgements

The authors would like to acknowledge the financial support of the National Natural Science Foundation of China (51603075; 21604026), and the support of the following two grants from Research Grants Council of Hong Kong. 1) “Proactive monitoring of work-

related MSD risk factors and fall risks of construction workers using wearable insoles" (PolyU 152099/18E); and 2) In search of a suitable tool for proactive physical fatigue assessment: an invasive to non-invasive approach. (PolyU 15204719/18E).

References

1. C. S. Wu, A. C. Wang, W. B. Ding, H. Y. Guo and Z. L. Wang, *Adv. Energy Mater.*, 2019, **9**.
2. Z. L. Wang, J. Chen and L. Lin, *Energ Environ Sci*, 2015, **8**, 2250-2282.
3. Z. L. Wang, *Acs Nano*, 2013, **7**, 9533-9557.
4. K. Parida, J. Q. Xiong, X. R. Zhou and P. S. Lee, *Nano Energy*, 2019, **59**, 237-257.
5. G. Zhu, Y. S. Zhou, P. Bai, X. S. Meng, Q. Jing, J. Chen and Z. L. Wang, *Adv Mater*, 2014, **26**, 3788-3796.
6. Y. Zhou, M. Zhang, Z. Guo, L. Miao, S. T. Han, Z. Wang, X. Zhang, H. Zhang and Z. Peng, *Materials Horizons*, 2017, **4**, 997-1019.
7. B. Meng, W. Tang, Z. H. Too, X. S. Zhang, M. D. Han, W. Liu and H. X. Zhang, *Energ Environ Sci*, 2013, **6**, 3235-3240.
8. Y. Lee, S. H. Cha, Y. W. Kim, D. Choi and J. Y. Sun, *Nat Commun*, 2018, **9**.
9. L. J. Sun, S. Chen, Y. F. Guo, J. C. Song, L. Z. Zhang, L. J. Xiao, Q. B. Guan and Z. W. You, *Nano Energy*, 2019, **63**.
10. D. W. Shin, M. D. Barnes, K. Walsh, D. Dimov, P. Tian, A. I. S. Neves, C. D. Wright, S. M. Yu, J. B. Yoo, S. Russo and M. F. Craciun, *Adv. Mater.*, 2018, **30**.
11. H. Y. Mi, X. Jing, Z. Y. Cai, Y. J. Liu, L. S. Turng and S. Q. Gong, *Nanoscale*, 2018, **10**, 23131-23140.
12. C. Yao, X. Yin, Y. Yu, Z. Cai and X. Wang, *Adv. Funct. Mater.*, 2017, **27**, 1700794.
13. B. K. Yun, J. W. Kim, H. S. Kim, K. W. Jung, Y. Yi, M. S. Jeong, J. H. Ko and J. H. Jung, *Nano Energy*, 2015, **15**, 523-529.
14. H. Ryu, J. H. Lee, T. Y. Kim, U. Khan, J. H. Lee, S. S. Kwak, H. J. Yoon and S. W. Kim, *Adv. Energy Mater.*, 2017, **7**.
15. H. Chu, H. Jang, Y. Lee, Y. Chae and J. H. Ahn, *Nano Energy*, 2016, **27**, 298-305.
16. G. Z. Li, G. G. Wang, D. M. Ye, X. W. Zhang, Z. Q. Lin, H. L. Zhou, F. Li, B. L. Wang and J. C. Han, *Adv Electron Mater*, 2019, **5**.
17. V. Harnchana, H. V. Ngoc, W. He, A. Rasheed, H. Park, V. Amornkitbamrung and D. J. Kang, *ACS Appl. Mater. Interfaces*, 2018, **10**, 25263-25272.
18. Y. C. Mao, D. L. Geng, E. J. Liang and X. D. Wang, *Nano Energy*, 2015, **15**, 227-234.
19. M. Wang, N. Zhang, Y. Tang, H. Zhang, C. Ning, L. Tian, W. Li, J. Zhang, Y. Mao and E. Liang, *J. Mater. Chem. A*, 2017, **24**, 12252-12257.
20. J. H. Shi, X. P. Chen, G. F. Li, N. Sun, H. X. Jiang, D. Q. Bao, L. J. Xie, M. F. Peng, Y. N. Liu, Z. Wen and X. H. Sun, *Nanoscale*, 2019, **11**, 7513-7519.
21. X. N. Xia, J. Chen, G. L. Liu, M. S. Javed, X. Wang and C. G. Hu, *Carbon*, 2017, **111**, 569-576.
22. X. W. Liang, T. Zhao, W. Jiang, X. C. Yu, Y. G. Hu, P. L. Zhu, H. R. Zheng, R. Sun and C. P. Wong, *Nano Energy*, 2019, **59**, 508-516.
23. J. M. Sun, X. Pu, M. M. Liu, A. F. Yu, C. H. Du, J. Y. Zhai, W. G. Hu and Z. L. Wang, *Acs Nano*, 2018, **12**, 6147-6155.
24. J. H. Park, G. T. Hwang, S. Kim, J. Seo, H. J. Park, K. Yu, T. S. Kim and K. J. Lee, *Adv. Mater.*, 2017, **29**.

25. C. Keplinger, J. Y. Sun, C. C. Foo, P. Rothemund, G. M. Whitesides and Z. G. Suo, *Science*, 2013, **341**, 984-987.
26. X. Jing, H. Y. Mi, Y. J. Lin, E. Enriquez, X. F. Peng and L. S. Turng, *ACS Appl. Mater. Interfaces*, 2018, **10**, 20897-20909.
27. X. Jing, H. Li, H. Y. Mi, Y. J. Liu, P. Y. Feng, Y. M. Tan and L. S. Turng, *Sensor Actuat B-Chem*, 2019, **295**, 159-167.
28. X. Pu, M. Liu, X. Chen, J. Sun, C. H. Du, Y. Zhang, J. Zhai, W. Hu and Z. L. Wang, *Science Advances*, 2017, **3**, e1700015.
29. K. Parida, V. Kumar, J. X. Wang, V. Bhavanasi, R. Bendi and P. S. Lee, *Adv. Mater.*, 2017, **29**.
30. G. R. Zhao, Y. W. Zhang, N. Shi, Z. R. Liu, X. D. Zhang, M. Q. Wu, C. F. Pan, H. L. Liu, L. L. Li and Z. L. Wang, *Nano Energy*, 2019, **59**, 302-310.
31. T. Liu, M. M. Liu, S. Dou, J. M. Sun, Z. F. Cong, C. Y. Jiang, C. H. Du, X. Pu, W. G. Hu and Z. L. Wang, *Acs Nano*, 2018, **12**, 2818-2826.
32. S. Xu, Y. H. Zhang, J. Cho, J. Lee, X. Huang, L. Jia, J. A. Fan, Y. W. Su, J. Su, H. G. Zhang, H. Y. Cheng, B. W. Lu, C. J. Yu, C. Chuang, T. I. Kim, T. Song, K. Shigeta, S. Kang, C. Dagdeviren, I. Petrov, P. V. Braun, Y. G. Huang, U. Paik and J. A. Rogers, *Nat Commun*, 2013, **4**.
33. Y. Qian, J. H. Nie, X. Ma, Z. W. Ren, J. W. Tian, J. Y. Chen, H. L. Shen, X. Y. Chen and Y. F. Li, *Nano Energy*, 2019, **60**, 493-502.
34. L. Y. Wang and W. A. Daoud, *Adv. Energy Mater.*, 2019, **9**.
35. H. Zhao, W. She, D. Shi, W. Wu, Q. C. Zhang and R. K. Y. Li, *Compos Part B-Eng*, 2019, **177**.
36. R. Iqbal, B. Majhy and A. K. Sen, *ACS Appl. Mater. Interfaces*, 2017, **9**, 31170-31180.
37. H. Yuk, T. Zhang, G. A. Parada, X. Liu and X. Zhao, *Nat Commun*, 2016, **7**, 12028.
38. M. H. Schneider, Y. Tran and P. Tabeling, *Langmuir*, 2011, **27**, 1232-1240.
39. H. Y. Mi, X. Jing, Q. Zheng, L. Fang, H. X. Huang, L. S. Turng and S. Gong, *Nano Energy*, 2018, **48**, 327-336.
40. B. U. Ye, B. J. Kim, J. Ryu, J. Y. Lee, J. M. Baik and K. Hong, *Nanoscale*, 2015, **7**, 18343-18343.
41. X. Y. Chen, Y. L. Wu, J. J. Shao, T. Jiang, A. F. Yu, L. Xu and Z. L. Wang, *Small*, 2017, **13**.
42. H. Y. Mi, X. Jing, M. A. B. Meador, H. Q. Guo, L. S. Turng and S. Q. Gong, *ACS Appl. Mater. Interfaces*, 2018, **10**, 30596-30606.
43. Q. B. Guan, G. H. Lin, Y. Z. Gong, J. F. Wang, W. Y. Tan, D. Q. Bao, Y. N. Liu, Z. W. You, X. H. Sun, Z. Wen and Y. Pan, *J. Mater. Chem. A*, 2019, **7**, 13948-13955.
44. P. Cui, K. Parida, M. F. Lin, J. Q. Xiong, G. F. Cai and P. S. Lee, *Adv. Mater. Interfaces*, 2017, **4**.
45. F. R. Fan, J. J. Luo, W. Tang, C. Y. Li, C. P. Zhang, Z. Q. Tian and Z. L. Wang, *J. Mater. Chem. A*, 2014, **2**, 13219-13225.
46. S. Kim, M. K. Gupta, K. Y. Lee, A. Sohn, T. Y. Kim, K. S. Shin, D. Kim, S. K. Kim, K. H. Lee, H. J. Shin, D. W. Kim and S. W. Kim, *Adv. Mater.*, 2014, **26**, 3918-3925.
47. B. Dudem, Y. H. Ko, J. W. Leem, S. H. Lee and J. S. Yu, *ACS Appl. Mater. Interfaces*, 2015, **7**, 20520-20529.
48. F. R. Fan, L. Lin, G. Zhu, W. Z. Wu, R. Zhang and Z. L. Wang, *Nano Lett.*, 2012, **12**, 3109-3114.
49. Y. H. Ko, G. Nagaraju, S. H. Lee and J. S. Yu, *ACS Appl. Mater. Interfaces*, 2014, **6**, 6631-6637.
50. B. D. Chen, W. Tang, T. Jiang, L. P. Zhu, X. Y. Chen, C. He, L. Xu, H. Y. Guo, P. Lin, D. Li, J. J. Shao and Z. L. Wang, *Nano Energy*, 2018, **45**, 380-389.